Mechanics of Advanced Composite Structures 3 (2016) 15-30

Semnan University

Mechanics of Advanced Composite Structures

journal homepage: http://macs.journals.semnan.ac.ir

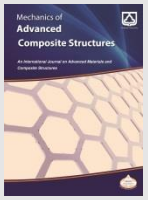

Dynamic Stiffness Method for Free Vibration of Moderately Thick Functionally Graded Plates

M. Soltani[a], S. Hatami[a,*], M. Azhari[b], H.R. Ronagh[c]

[a]*Department of Civil Engineering, Yasouj University, Yasouj, Iran*

[b]*Department of Civil Engineering, Isfahan University of Technology, Isfahan, Iran*

[c]*Institute for Infrastructure Engineering, Western Sydney University, Sydney, Australia*

PAPER INFO

Paper history:
Received 2015-11-27
Revision Received 2016-04-29
Accepted 2016-05-08

Keywords:
Dynamic stiffness method
Free vibration
Functionally graded material
First-order shear deformation theory
Exact solution

ABSTRACT

In this study, a dynamic stiffness method for free vibration analysis of moderately thick functionally graded material plates is developed. The elasticity modulus and mass density of the plate are assumed to vary according to a power-law distribution in terms of the volume fractions of the constituents whereas Poisson's ratio is constant. Due to the variation of the elastic properties through the thickness, the equations of motion governing the in-plane and transverse deformations are initially coupled. Using a new reference plane instead of the mid-plane of the plate, the uncoupled differential equations of motions are derived. The out-of-plane equations of motion are solved by introducing the auxiliary and potential functions and using the separation of variables method. Using the method, the exact natural frequencies of the Functionally Graded Plates (FGPs) are obtained for different boundary conditions. The accuracy of the natural frequencies obtained from the present dynamic stiffness method is evaluated by comparing them with those obtained from the methods suggested by other researchers.

1. Introduction

Functionally Graded Materials (FGMs) are inhomogeneous composites made from different phases of material constituents (usually ceramic and metal). The FGMs were initially designed as thermal barriers for aerospace structures and fusion reactors. In the plate form the Functionally Graded Plates (FGPs) are widely used in structural applications and their behaviour has been studied by several investigators. Mizuguchi and Ohnabe [1] used Galerkin method to analyse a clamped rectangular plate subjected to an arbitrary symmetrical temperature and a load distribution about the midpoint of the plate, while the plate was prevented from in-plane motions on the boundaries. Parveen and Reddy investigated the response of functionally graded ceramic metal plates using a finite element technique that accounted for the transverse shear strains, rotary inertia and moderately large rotations. The static and dynamic responses of the FGPs were investigated by varying the volume fraction of the ceramic and metallic constituents using a simple power law distribution [2]. In this regard, Yang and Shen dealt with the dynamic response of initially stressed functionally graded rectangular thin plates subjected to partially distribute impulsive lateral loads resting on an elastic foundation [3]. Then, they analysed free and forced vibration for initially stressed FGPs in thermal environment [4]. The third-order shear deformation plate theory was employed to solve the axisymmetric bending and buckling problems of functionally graded circular plates by Ma and Wang [5]. Kitipornchai et al. [6] investigated the nonlinear vibration of imperfect shear deformable laminated rectangular plates comprising a homogeneous substrate and two layers of FGMs. The thermal buckling of circular plates composed of FGMs was considered by Najafizadeh and Heydari [7]. A recently developed plate theory using the concept of shape function of the transverse coordinate parameter was extended to determine the stress distribution in an orthotropic FGP subjected

* Corresponding author, Tel.: +98-743-1005118; Fax: +98-743-3221711

E-mail address: hatami@yu.ac.ir

to the cylindrical bending by Bian et al. [8]. Based on the three-dimensional fundamental equations of anisotropic elasticity, a state equation with variable coefficients was derived in a unified matrix form by Chen et al. [9]. The free vibration analysis of arbitrary shaped thick plates by differential cubature method was analysed by Wu and Liu [10]. Abrate [11] investigated a functionally graded isotropic elastic rectangular plate with in-plane material inhomogeneity. An closed-form procedure was proposed by Hosseini-Hashemi et al. [12] for the free vibration analysis of moderately thick rectangular plates simply supported at the two opposite edges (i.e. Levy-type rectangular plates). Their procedure was based on the Reissner–Mindlin plate theory. Then, Hosseini-Hashemi et al. [13] worked on free vibration analysis of moderately thick rectangular plates, which were composed of functionally graded materials and supported by either Winkler or Pasternik elastic foundations.

The finite element based simulation of the dynamic response is regularly employed by the FGM manufacturers in order to improve their products' comfort and reliability. For instance, the asymmetric free vibration characteristics and thermo-elastic stability of functionally graded circular plates were investigated using finite element procedure by Parkash and Ganapathi [14]. Shariyat [15] analysed the vibration and dynamic buckling of functionally graded rectangular plates using a finite element formulation based on a higher-order shear deformation theory. Afsar and Go [16] focused on the finite element analysis of thermo-elastic field in a thin circular FGM disk subjected to a thermal load and an inertia force due to the rotation of the disk. Moreover, the large amplitude flexural vibration characteristics of FGPs were investigated by Parkash et al. [17] using a shear flexible Finite Element Method (FEM). The FEM is a powerful tool to analyse a complex geometry of modelled structures which is essential for industrial applications. However, with high-frequency excitation, many structures of interest require very large computer models which reduce the computational efficiency when the finite element technique is used for discretization. Hence, for specific geometries, periodic or semi-infinite boundary conditions, the frequency domain methods such as dynamic stiffness matrix, strip element and spectral finite element were developed to overcome the problem.

Among the frequency domain methods, Dynamic Stiffness Method (DSM) is very suitable for solving dynamic problems. The method is often referred to as an exact method as it is based on exact shape functions obtained from the solution of the differential equations of motion. The DSM, which yields exact results for certain class of plate structures, is used to analyse free vibration frequencies of various structures. Leung and Fung [18] extended the DSM to a large amplitude free and forced vibration of frames. A general theory to develop the dynamic stiffness matrix of a structural element has been outlined by Banerjee [19]. A direct-DSM was presented for the vibration analysis of orthotropic plate structures by Bercin [20]. Bercin and Langley [21] extended the DSM to include in-plane vibrations of the plate. The direct-DSM was extended to the vibration analysis of Mindlin plates by Bercin, then investigated the effects of shear distortion and rotary inertia on the flexural energy transmission of a representative stiffened plate structure [22]. Later, Bercin employs the DSM to calculate the free vibration of various simply-supported plate and sees that while for the directly coupled plate assemblies the in-plane effects are negligible for low-order modes, for the stiffened plate assembly the effect of in-plane motion equals a reduction in the free vibration frequencies [23]. Application of the DSM to turbulent boundary layer was presented by Birgersson et al. [24]. Hatami and Azhari [25] formulated the DSM for orthotropic plates moving on some rollers and an elastic foundation. Boscolo and Banerjee [26] developed the DSM for plates based on the first-order shear deformation theory to carry out the exact free vibration analysis of the plate assemblies. In addition, the dynamic stiffness formulation for both in-plane and bending free vibration based on the first-order shear deformation theory for composite plates was presented by the same team [27]. They investigated the in-plane free vibration behaviour of plates using the DSM. Some distinctive modes which were unnoticed in earlier investigations using the DSM were addressed by revisiting the problem and focusing on the special set of missing solutions [28]. Then, The DSM for composite plate elements based on the first-order shear deformation theory was implemented in a program called DySAP that computed the exact natural frequencies and mode shapes of composite structures by them [29]. Based on a higher order shear deformation theory, Fazzolari et al. [30] developed an DSM in order to carry out the free vibration analysis of composite plate assemblies. To derive the governing differential equations of motion and natural boundary conditions, they implemented Hamilton's principle. They used Wittrick–Williams algorithm [31] as a solution technique to compute the natural frequencies and mode shapes for a range of laminated composite plates and stepped panels. The dynamic stiffness matrix for isotropic rectangular plate with arbitrary boundary conditions undergoing in-plane free vibration was developed by Nefovska-Danilovic and Petronijevic [32]. An exact method for free vibration analysis of plates with arbitrary boundary conditions is presented by Liu and Banerjee [33] which the formulation satisfies the governing differential

equation exactly and any arbitrary boundary conditions are satisfied in a series sense.

In this study, the free vibration of moderately thick FGPs is studied by DSM using First-order Shear Deformation Theory (FSDT). Based on the knowledge of the authors, there are no studies available in the literature (including the articles reviewed in this section) developing dynamic stiffness matrices for FGPs using FSDT.

The basic characteristic of the "moderately thick" plate theories is that the rotations of plate cross sections cannot be merely expressed in terms of the transverse displacement. Thus, there exist three basic quantities at the plate edge including out-of-plane displacement and rotations. For solving the equations of motion by DSM, the potential functions presented by Bercin [22] are used to convert the three out-of-plane equations in to three independent equations. Solving these independent equations and composing the results of each equation, the dynamic stiffness matrix of a plate element is derived which allows the calculation of the free vibration frequencies of the moderately thick plate. Several cases dealing with free vibration problems are presented in order to illustrate the accuracy of results obtained by the suggested method.

2. Functionally Graded Materials

In the laminated composite plates, the stress concentrations generate along the interfaces, more specifically when high temperatures are involved. This can lead to delamination, matrix cracking and other damage mechanisms which result from the abrupt change of the mechanical properties at the interface of the layers. One way to overcome this problem is to use Functionally Graded Materials (FGMs) within which the material properties have continuous variation from one surface to the other.

The FGMs are composite materials, the mechanical properties of which vary continuously in the thickness direction. However, a detailed description of actual graded microstructure is usually not available, perhaps except for the volume fraction distribution. The FGMs are often manufactured by two phases of materials with different properties. Since the volume fraction of each phase gradually varies in the graded direction, the effective properties of the FGMs change along this direction, as shown in Fig. 1. In this study, a continuous variation is assumed for the volume fraction of ceramic or metal, and the metal volume fraction can be represented by the following function of the transverse coordinate *z*.

$$V_c = \left(\frac{z}{h}+\frac{1}{2}\right)^p, -(h/2) \le z \le +(h/2) \quad (1)$$

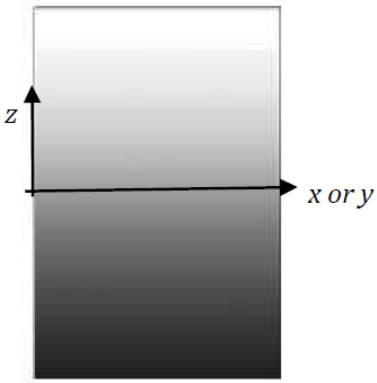

Figure 1. The schematic illustration of a two-phase FGM

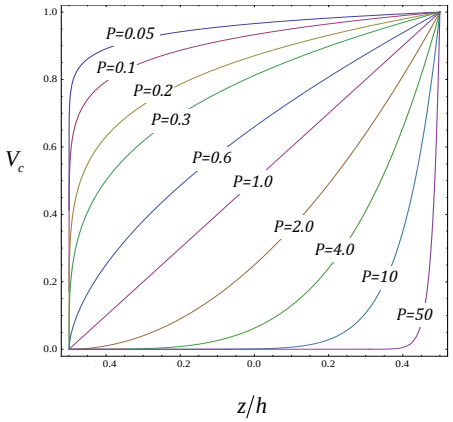

Figure 2. The variation of volume fraction through the dimensionless thickness of the plate

Where *h* is the thickness of the structure, and *P* $(0 \le P \le \infty)$ is a volume fraction exponent that denotes the material variation profile through the FGP thickness. As the variation of *P* is presented in Fig. 2, changing the value of *P* generates an infinite number of composition distributions.

$$T(z) = (T_c - T_m)V_c + T_m \quad (2)$$

Where the subscripts *m* and *c* refer to the metallic and ceramic constituents, respectively, and the material's property *T*, can be the modulus of the elasticity (E), the density (ρ), or the Poisson's ratio (ϑ).

3. Equations of Motion

According to the first-order shear deformation theory, the displacements of the plate are represented as the following [34]:

$$\begin{aligned} u(x,y,z,t) &= u_0(x,y,t) + z\phi_x(x,y,t) \\ v(x,y,z,t) &= v_0(x,y,t) + z\phi_y(x,y,t) \\ w(x,y,z,t) &= w_0(x,y,t) \end{aligned} \quad (3)$$

Where *u* and *v* are the in-plane displacements and *w*, ϕ_x and ϕ_y are the out-of plane displacements and rotations about y and x axes, respectively. The zero index identifies the mid-plane displacement along the *x*, *y* and *z* axes (Fig. 3).

The strains associated with the displacement field in Eq. (3) are given by the following equations:

$$\varepsilon_{xx} = \frac{\partial u_0}{\partial x} + z\frac{\partial \phi_x}{\partial x}$$

$$\varepsilon_{yy} = \frac{\partial v_0}{\partial y} + z\frac{\partial \phi_y}{\partial y}$$

$$\varepsilon_{zz} = 0 \tag{4}$$

$$\gamma_{xy} = \left(\frac{\partial u_0}{\partial y} + \frac{\partial v_0}{\partial x}\right) + z\left(\frac{\partial \phi_x}{\partial y} + \frac{\partial \phi_y}{\partial x}\right)$$

$$\gamma_{xz} = \frac{\partial w}{\partial x} + \phi_x$$

$$\gamma_{yz} = \frac{\partial w}{\partial y} + \phi_y$$

Note that the in-plane strains $\left(\varepsilon_{xx}, \varepsilon_{yy}, \gamma_{xy}\right)$ are linear through the plate thickness, while the transverse shear strains $\left(\gamma_{xz}, \gamma_{yz}\right)$ are constant. The strains in Eq. (4) can be expressed in the vector form as the following:

$$\begin{Bmatrix} \varepsilon_{xx} \\ \varepsilon_{yy} \\ \gamma_{xy} \end{Bmatrix} = \begin{Bmatrix} \varepsilon_{xx}^{(0)} \\ \varepsilon_{yy}^{(0)} \\ \gamma_{xy}^{(0)} \end{Bmatrix} + z\begin{Bmatrix} \varepsilon_{xx}^{(1)} \\ \varepsilon_{yy}^{(1)} \\ \gamma_{xy}^{(1)} \end{Bmatrix} \rightarrow$$

$$= \begin{Bmatrix} \dfrac{\partial u_0}{\partial x} \\ \dfrac{\partial v_0}{\partial y} \\ \dfrac{\partial u_0}{\partial y} + \dfrac{\partial v_0}{\partial x} \end{Bmatrix} + z\begin{Bmatrix} \dfrac{\partial \phi_x}{\partial x} \\ \dfrac{\partial \phi_y}{\partial y} \\ \dfrac{\partial \phi_x}{\partial y} + \dfrac{\partial \phi_y}{\partial x} \end{Bmatrix} \tag{5.a}$$

$$\begin{Bmatrix} \gamma_{yz} \\ \gamma_{xz} \end{Bmatrix} = \begin{Bmatrix} \gamma_{yz}^{(0)} \\ \gamma_{xz}^{(0)} \end{Bmatrix} = \begin{Bmatrix} \dfrac{\partial w}{\partial y} + \phi_y \\ \dfrac{\partial w}{\partial x} + \phi_x \end{Bmatrix} \tag{5.b}$$

The stresses resultant is related to the strains by the following expressions:

$$\begin{Bmatrix} \sigma_{xx} \\ \sigma_{yy} \\ \sigma_{xy} \end{Bmatrix} = \begin{bmatrix} Q_{11} & Q_{12} & 0 \\ Q_{21} & Q_{22} & 0 \\ 0 & 0 & Q_{66} \end{bmatrix} \begin{Bmatrix} \varepsilon_{xx} \\ \varepsilon_{yy} \\ \gamma_{xy} \end{Bmatrix},$$

$$\begin{Bmatrix} \tau_{yz} \\ \tau_{xz} \end{Bmatrix} = \begin{bmatrix} Q_{44} & 0 \\ 0 & Q_{55} \end{bmatrix} \begin{Bmatrix} \gamma_{yz} \\ \gamma_{xz} \end{Bmatrix} \tag{6}$$

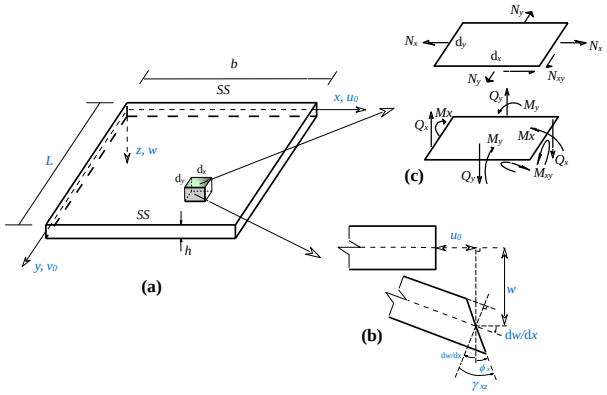

Figure 3. A rectangular moderately thick plate, a) coordinate system of the plate, b) deformation of the plate section, c) in-plane and out-of-plane forces on an infinitesimal element of the plate

Where Q_{ii} is referred to as the reduced stiffness component. For an isotropic FGM plate they are obtained as what follow:

$$Q_{11} = Q_{22} = \frac{E(z)}{\left(1-\vartheta^2(z)\right)},$$

$$Q_{12} = \vartheta(z)Q_{11}, Q_{66} = \frac{E(z)}{2\left(1+\vartheta(z)\right)}, \tag{7}$$

$$Q_{44} = Q_{55} = G(z)$$

Where ϑ and G are Poisson's ratio and shear modules, respectively. The forces and moment resultants are defined by Eq. 8 as follows:

$$\begin{Bmatrix} \boldsymbol{N} \\ \boldsymbol{M} \end{Bmatrix} = \begin{bmatrix} \boldsymbol{A} & \boldsymbol{B} \\ \boldsymbol{B} & \boldsymbol{D} \end{bmatrix} \begin{Bmatrix} \boldsymbol{\varepsilon}^{(0)} \\ \boldsymbol{\varepsilon}^{(1)} \end{Bmatrix},$$

$$\boldsymbol{Q} = \begin{bmatrix} A_{44} & 0 \\ 0 & A_{55} \end{bmatrix} \begin{Bmatrix} \dfrac{\partial w}{\partial y} + \phi_y \\ \dfrac{\partial w}{\partial x} + \phi_x \end{Bmatrix} \tag{8}$$

Where $\boldsymbol{N}$, $\boldsymbol{M}$ and $\boldsymbol{Q}$ are the vectors of in-plane forces, moments and transverse shear forces, respectively as follows:

$$\boldsymbol{N} = \begin{Bmatrix} N_x \\ N_y \\ N_{xy} \end{Bmatrix}, \quad \boldsymbol{M} = \begin{Bmatrix} M_x \\ M_y \\ M_{xy} \end{Bmatrix}, \tag{9}$$

$$\boldsymbol{Q} = \begin{Bmatrix} Q_y \\ Q_x \end{Bmatrix}$$

And A_{ij} ($i,j=4,5$), are the shear stiffness resultants defined as the following:

$$\begin{Bmatrix} A_{44} \\ A_{55} \end{Bmatrix} = \int_{-h/2}^{h/2} k_s^2 \begin{Bmatrix} Q_{44} \\ Q_{55} \end{Bmatrix} \mathrm{d}z \tag{10}$$

For isotropic materials, there is no coupling between the shear deformations in two directions, i.e., $A_{45}=0$ and $A_{44}=A_{55}$. Therefore, it is sufficient to identify only one of the components A_{44} or A_{55}. The shear correction factor k_s^2, is assumed to be $5/6$ [34]. The components of extensional (A), coupling (B) and bending (D) stiffness matrices in Eq. 9 are defined as the following:

$$\left(A_{ij}, B_{ij}, D_{ij}\right) = \int_{-h/2}^{h/2} Q_{ij}\left(1, z, z^2\right) \mathrm{d}z, \quad i, j = 1,\ 2 \text{ and } 6 \tag{11}$$

Using the Hamilton's principle [34], and eliminating first moment of inertia, the equations of motion in terms of forces and moment resultants are governed by the following relations:

$$\frac{\partial N_x}{\partial x} + \frac{\partial N_{xy}}{\partial y} = I_0 \frac{\partial^2 u_0}{\partial t^2} \tag{12.a}$$

$$\frac{\partial N_{xy}}{\partial x} + \frac{\partial N_y}{\partial y} = I_0 \frac{\partial^2 v_0}{\partial t^2} \tag{12.b}$$

$$\frac{\partial Q_x}{\partial x} + \frac{\partial Q_y}{\partial y} = I_0 \frac{\partial^2 w}{\partial t^2} \tag{12.c}$$

$$\frac{\partial M_x}{\partial x} + \frac{\partial M_{xy}}{\partial y} - Q_x = I_2 \frac{\partial^2 \phi_x}{\partial t^2} \tag{12.d}$$

$$\frac{\partial M_{xy}}{\partial x} + \frac{\partial M_y}{\partial y} - Q_y = I_2 \frac{\partial^2 \phi_y}{\partial t^2} \tag{12.e}$$

In which

$$\left\{I_0, I_2\right\} = \int_{-h/2}^{h/2} \rho(z)\left\{1, z^2\right\} \mathrm{d}z \tag{13}$$

Where I_0 and I_2 are the mass of the plate per unit area and its mass moment of inertia, respectively. The density, $\rho(z)$, can potentially vary through the thickness.

Substituting Eqs. (5) and (8) to Eqs. (12a-12e), the equations of motion for a rectangular moderately thick FGM plate, based on the mid-plane displacements are obtained as what follow:

$$\begin{aligned}
&A_{11}\frac{\partial^2 u_0}{\partial x^2} + A_{12}\frac{\partial^2 v_0}{\partial x\,\partial y} + \\
&A_{16}\left(2\frac{\partial^2 u_0}{\partial x\,\partial y} + \frac{\partial^2 v_0}{\partial x^2}\right) + \\
&A_{26}\frac{\partial^2 v_0}{\partial y^2} + A_{66}\left(\frac{\partial^2 v_0}{\partial x\,\partial y} + \frac{\partial^2 u_0}{\partial y^2}\right) + \\
&B_{11}\frac{\partial^2 \phi_x}{\partial x^2} + B_{12}\frac{\partial^2 \phi_y}{\partial x\,\partial y} + \\
&B_{16}\left(2\frac{\partial^2 \phi_x}{\partial x\,\partial y} + \frac{\partial^2 \phi_y}{\partial x^2}\right) + B_{26}\frac{\partial^2 \phi_y}{\partial y^2} + \\
&B_{66}\left(\frac{\partial^2 \phi_y}{\partial x\,\partial y} + \frac{\partial^2 \phi_x}{\partial y^2}\right) = I_0\frac{\partial^2 u_0}{\partial t^2}
\end{aligned} \tag{14.a}$$

$$\begin{aligned}
&A_{12}\frac{\partial^2 u_0}{\partial x\,\partial y} + A_{22}\frac{\partial^2 v_0}{\partial y^2} + A_{16}\frac{\partial^2 u_0}{\partial x^2} + \\
&A_{26}\left(2\frac{\partial^2 v_0}{\partial x\,\partial y} + \frac{\partial^2 u_0}{\partial y^2}\right) + \\
&A_{66}\left(\frac{\partial^2 u_0}{\partial x\,\partial y} + \frac{\partial^2 v_0}{\partial x^2}\right) + \\
&B_{12}\frac{\partial^2 \phi_x}{\partial x\,\partial y} + B_{22}\frac{\partial^2 \phi_y}{\partial y^2} + \\
&B_{16}\frac{\partial^2 \phi_x}{\partial x^2} + B_{26}\left(2\frac{\partial^2 \phi_y}{\partial x\,\partial y} + \frac{\partial^2 \phi_x}{\partial y^2}\right) + \\
&B_{66}\left(\frac{\partial^2 \phi_x}{\partial x\,\partial y} + \frac{\partial^2 \phi_y}{\partial x^2}\right) = I_0\frac{\partial^2 v_0}{\partial t^2}
\end{aligned} \tag{14.b}$$

$$\begin{aligned}
&A_{55}\left(\frac{\partial^2 w}{\partial x^2} + \frac{\partial \phi_x}{\partial x}\right) + \\
&A_{44}\left(\frac{\partial^2 w}{\partial y^2} + \frac{\partial \phi_y}{\partial y}\right) = I_0\frac{\partial^2 w}{\partial t^2}
\end{aligned} \tag{14.c}$$

$$
\begin{aligned}
&B_{11}\frac{\partial^2 u_0}{\partial x^2}+B_{12}\frac{\partial^2 v_0}{\partial x\,\partial y}+\\
&B_{16}\left(2\frac{\partial^2 u_0}{\partial x\,\partial y}+\frac{\partial^2 v_0}{\partial x^2}\right)+\\
&B_{26}\frac{\partial^2 v_0}{\partial y^2}+B_{66}\left(\frac{\partial^2 u_0}{\partial y^2}+\frac{\partial^2 v_0}{\partial y\,\partial x}\right)+\\
&D_{11}\frac{\partial^2 \phi_x}{\partial x^2}+D_{12}\frac{\partial^2 \phi_y}{\partial x\,\partial y}+\\
&D_{16}\left(2\frac{\partial^2 \phi_x}{\partial x\,\partial y}+\frac{\partial^2 \phi_y}{\partial x^2}\right)+\\
&D_{26}\frac{\partial^2 \phi_y}{\partial y^2}+D_{66}\left(\frac{\partial^2 \phi_x}{\partial y^2}+\frac{\partial^2 \phi_y}{\partial x\,\partial y}\right)\\
&-A_{55}\left(\frac{\partial w}{\partial x}+\phi_x\right)=I_2\frac{\partial^2 \phi_x}{\partial t^2}
\end{aligned}
\tag{14.d}
$$

$$
\begin{aligned}
&B_{12}\frac{\partial^2 u_0}{\partial x\,\partial y}+B_{22}\frac{\partial^2 v_0}{\partial y^2}+\\
&B_{26}\left(2\frac{\partial^2 v_0}{\partial x\,\partial y}+\frac{\partial^2 u_0}{\partial y^2}\right)+\\
&B_{16}\frac{\partial^2 u_0}{\partial x^2}+B_{66}\left(\frac{\partial^2 v_0}{\partial x^2}+\frac{\partial^2 u_0}{\partial y\,\partial x}\right)+\\
&D_{12}\frac{\partial^2 \phi_x}{\partial x\,\partial y}+D_{22}\frac{\partial^2 \phi_y}{\partial y^2}+\\
&D_{26}\left(2\frac{\partial^2 \phi_y}{\partial x\,\partial y}+\frac{\partial^2 \phi_x}{\partial y^2}\right)+\\
&D_{16}\frac{\partial^2 \phi_x}{\partial x^2}+D_{66}\left(\frac{\partial^2 \phi_y}{\partial x^2}+\frac{\partial^2 \phi_x}{\partial x\,\partial y}\right)\\
&-A_{44}\left(\frac{\partial w}{\partial y}+\phi_y\right)=I_2\frac{\partial^2 \phi_y}{\partial t^2}
\end{aligned}
\tag{14.e}
$$

Even when in-plane inertias are ignored, these equations of motion (Eqs. 14) show that in-plane and out-of-plane are coupled. Nevertheless, Abrate [35] shows that the equations of motion can be uncoupled if a different reference surface rather than the mid-plane of plate is selected. He uses a new reference plane ($z'=0$) with a distance of δ from mid-plane ($z=0$), as shown in Fig. 4. The distance is calculated as the elements of the coupling matrix are zero according to the new reference surface.

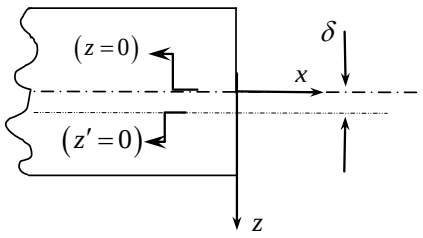

Figure 4. The new coordinate system (z') which $B'_{ij}=0$

To obtain the stiffness properties of the plate according to the new reference plane (A'_{ij},B'_{ij},D'_{ij}), as proposed by Abrate [35], z is replaced with $z'+\delta$ in Eq. (11); then, we have the following:

$$A_{ij}=\int_{-h/2}^{h/2}Q_{ij}\,dz=\int_{-z'_b}^{z'_t}Q_{ij}\,dz'=A'_{ij} \tag{15}$$

$$
\begin{aligned}
B_{ij}&=\int_{-h/2}^{h/2}Q_{ij}\,z\,dz=\int_{-z'_b}^{z'_t}Q_{ij}\left(z'+\delta\right)dz'=\\
&\int_{-z'_b}^{z'_t}Q_{ij}\,z'\,dz'+\delta\int_{-z'_b}^{z'_t}Q_{ij}\,dz'=B'_{ij}+\delta A'_{ij}
\end{aligned}
\tag{16}
$$

Eqs. (15) and (16) yield what follows:

$$B'_{ij}=B_{ij}-\delta A_{ij} \tag{17}$$

Also

$$
\begin{aligned}
D_{ij}&=\int_{-z'_b}^{z'_t}Q_{ij}\left(z'+\delta\right)^2dz'=\\
&\int_{-z'_b}^{z'_t}Q_{ij}\left(z'^2+\delta^2+2z'\delta\right)dz'=\\
&D'_{ij}+2\delta B'_{ij}+\delta^2A'_{ij}
\end{aligned}
\tag{18}
$$

Using Eqs. (15), (17) and (18) we can obtain the following:

$$D'_{ij}=D_{ij}-2\delta B'_{ij}-\delta^2A_{ij} \tag{19}$$

or $$D'_{ij}=D_{ij}-2\delta B_{ij}+\delta^2A_{ij} \tag{20}$$

Where z'_t and z'_b are the values of z' on the top and bottom surfaces of the plate, respectively. A_{ij} and A'_{ij} are equal, because both of A_{ij} and A'_{ij} are the area under Q_{ij} function when z or z' varies along the plate thickness.

Setting B'_{ij} in Eq. (17) to zero, the distance of the mid-plane to the new plane is $\delta=B_{ij}/A_{ij}$. δ is not dependent on ij subscript in the case of constant Poisson's ratio. In this case, all elements of B' become zero only with a single δ. Even though the Poisson's ratio varies along the plate thickness, by considering $\delta=B_{11}/A_{11}$; B'_{11}, B'_{22}, B'_{12} and B'_{66} also become small amounts.

So, substituting $B'_{ij}=0$ and $\delta=B_{ij}/A_{ij}$ into Eq. (19), D'_{ij} can be rewritten as follows:

$$D'_{ij}=D_{ij}-\delta^2 A_{ij}=D_{ij}-\frac{B_{ij}^{\ 2}}{A_{ij}} \tag{21}$$

Using Eqs. (11) and (21), the following relations are obtained for the elements of D'_{ij} :

$$D'_{11}=D'_{22}=\left(D'_{12}+2D'_{66}\right)=D'_0 \tag{22.a}$$

$$D'_{16}=D'_{26}=0 \tag{22.b}$$

In which D'_0 is just introduced for simplicity of the notations.

Using flexural rigidity around new reference plane from Eqs. (22) and setting B'_{ij} to zero, Eq. (8) gives us the bending moments around the new reference plane. Replacing those bending moments into Eqs. (12 c, d, e), out of plane free vibration differential equations for a moderately thick FGM are obtained as follows:

$$k_s^{\ 2}Gh\left(\nabla^2 w+\Phi\right)-I_0\frac{\partial^2 w}{\partial t^2}=0 \tag{23.a}$$

$$\frac{1}{2}D'_o\left[\left(1-\vartheta\right)\nabla^2\phi_x+\left(1+\vartheta\right)\frac{\partial\Phi}{\partial x}\right]$$

$$-k_s^{\ 2}Gh\left(\phi_x+\frac{\partial w}{\partial x}\right) \tag{23.b}$$

$$-I_2\frac{\partial^2\phi_x}{\partial t^2}=0$$

$$\frac{1}{2}D'_o\left[\left(1-\vartheta\right)\nabla^2\phi_y+\left(1+\vartheta\right)\frac{\partial\Phi}{\partial y}\right]$$

$$-k_s^{\ 2}Gh\left(\phi_y+\frac{\partial w}{\partial y}\right) \tag{23.c}$$

$$-I_2\frac{\partial^2\phi_y}{\partial t^2}=0$$

In these relations, $\Phi=\partial\phi_x/\partial x+\partial\phi_y/\partial y$ and $\nabla^2=\partial^2/\partial x^2+\partial^2/\partial y^2$.

The basic characteristic of "moderately thick" plate theories is that the rotations ϕ_x and ϕ_y (Fig. 5) of the plate cross sections about the in-plane coordinate axes *x* and *y* cannot be merely expressed in terms of the normal deflection *w*. Thus, there exist three basic quantities ϕ_y, ϕ_x and *w* (transverse displacement) at the plate edge rather than just *w* as in the thin plate theory. So, for solving the equations of motion presented in Eqs. (23.a, b, c) by DSM, there is a need to uncouple these equations. Introducing some potential functions, Mindlin [36] developed a method for uncoupling such equations. Using the Mindlin method and the formulation presented by Bercin [22], Eqs. (23) can be written as the following:

$$\left(\nabla^2+\psi_1^2\right)W_1=0 \tag{24.a}$$

$$\left(\nabla^2+\psi_2^2\right)W_2=0 \tag{24.b}$$

$$\left(\nabla^2+\psi_3^2\right)H=0 \tag{24.c}$$

Where W_1, W_2 and *H* are potential functions. ψ_1, ψ_2 and ψ_3 represent the wave numbers, which are given by the following equations:

$$\psi_1^2,\psi_2^2=\frac{1}{2}\eta^4 \times\left[\left(S+R\right)\pm\sqrt{\left(S-R\right)^2+\frac{4}{\eta^4}}\right] \tag{25}$$

$$\psi_3^2=\frac{2}{1-\vartheta}\left(S\eta^4-\frac{1}{R}\right) \tag{26}$$

Where $S=h^2/12$, $R=D'_o/k_s^{\ 2}Gh$, and η is the classical plate flexural wave number defined as what follows:

$$\eta=\left(\frac{\rho h\omega^2}{D'_o}\right)^{\frac{1}{4}} \tag{27}$$

The rotations ϕ_x and ϕ_y, and the normal deflection *w* are calculated from the potential functions as the following:

$$\phi_x=\left(\Gamma_1-1\right)\frac{\partial W_1}{\partial x}+\left(\Gamma_2-1\right)\frac{\partial W_2}{\partial x}+\frac{\partial H}{\partial y}$$

$$\phi_y=\left(\Gamma_1-1\right)\frac{\partial W_1}{\partial y}+\left(\Gamma_2-1\right)\frac{\partial W_2}{\partial y}+\frac{\partial H}{\partial x} \tag{28}$$

$$w=W_1+W_2$$

In which

$$\Gamma_1=\frac{R\eta^4}{\psi_1^2},\quad \Gamma_2=\frac{R\eta^4}{\psi_2^2} \tag{29}$$

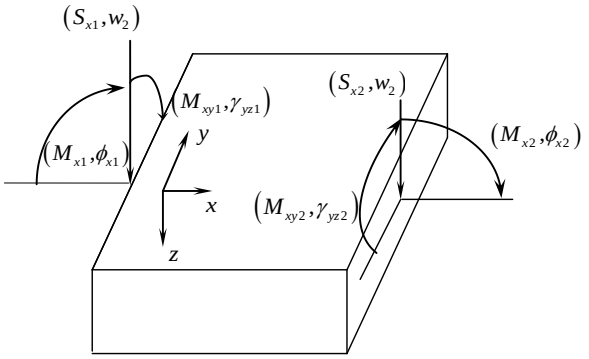

Figure 5. Nodal displacement and forces acting on the edges of a thick plate element

4. Dynamic Stiffness Method

The DSM is similar to the FEM in that the structure is discretised into the number of elements or substructures at the natural structural boundaries. Since the mode shape of a member varies with the vibration frequency, the FEM requires a subdivision of a structure into many finite elements for accurate solution of the free vibration equations. Alternatively, using the DSM in which the shape functions are frequency dependent, the exact solution is obtained employing only a few elements.

Fig. 3(a) shows a FGM rectangular plate with simple boundary conditions along the x direction. For such a plate, the general form of the three potential functions of Eqs. (24) may be expressed as the following[22]**:**

$$W_{1n}(x,y,t)=e^{i\omega t}\times \left(\tilde{A}_{1n}e^{r_n x}+\tilde{A}_{2n}e^{-r_n x}\right)\times \left(e^{ik_n y}-e^{-ik_n y}\right) \quad (30.a)$$

$$W_{2n}(x,y,t)=e^{i\omega t}\times \left(\tilde{B}_{1n}e^{\chi_n x}+\tilde{B}_{2n}e^{-\chi_n x}\right)\times \left(e^{ik_n y}-e^{-ik_n y}\right) \quad (30.b)$$

$$H_n(x,y,t)=e^{i\omega t}\times \left(\tilde{C}_{1n}e^{\mu_n x}+\tilde{C}_{2n}e^{-\mu_n x}\right)\times \left(e^{ik_n y}+e^{-ik_n y}\right) \quad (30.c)$$

$\tilde{A}_{mn}$, $\tilde{B}_{mn}$ and $\tilde{C}_{mn}$ *(m=1,2)* are coefficients of the equation solution, $k_n=n\pi/L$ is the wave number of the *n* th mode in *y* direction *(n=1,2,...)*, and ω is the frequency of vibration. Substituting Eq. (30) into Eq. (24), the problem then essentially becomes one-dimensional where r_n , χ_n and μ_n are given by the following equations:

$$r_n=\left(k_n^2-\psi_1^2\right)^{\frac{1}{2}},\quad \chi_n=\left(k_n^2-\psi_2^2\right)^{\frac{1}{2}},\quad \mu_n=\left(k_n^2-\psi_3^2\right)^{\frac{1}{2}} \quad (31)$$

Substituting Eqs. (30) into Eqs. (28) implies that the form of the potential functions satisfies the simple boundary conditions along the x direction i.e. the displacements $\left(\gamma_{yz},\phi_x,w\right)$ since vibration varies sinusoidally in the y -direction. Also, using Eqs. (5) and (8), it is evident the moments and transverse shear forces *(M_{xy}, M_x, Q_x)*, which are dependent on the displacements, vary sinusoidally in this direction. Satisfying the boundary conditions on two sides of the plate edges parallel to *y*-axis, the dynamic stiffness matrix of the element can be obtained. As shown in Fig. 5, these boundary conditions are what follow:

at $x=0$ (32)

$$\gamma_{yz}=\gamma_{yz1},\phi_x=\phi_{x1},w=w_1,$$
$$M_{xy}=M_{xy1},M_y=M_{y1},Q_x=S_{x1}$$

at $x=b$ (33)

$$\gamma_{yz}=\gamma_{yz2},\phi_x=\phi_{x2},w=w_2,$$
$$M_{xy}=M_{xy2},M_y=M_{y2},Q_x=S_{x2}$$

So, the edge displacements and forces vectors can be defined as the following:

$$\{d_n\}=\left\langle\gamma_{yz1n},\phi_{x1n},w_{1n},\gamma_{yz2n},\phi_{x2n},w_{2n}\right\rangle^T \quad (34)$$

$$\{p_n\}=\left\langle M_{xy1},M_{y1},S_{x1},M_{xy2},M_{y2},S_{x2}\right\rangle^T \quad (35)$$

Using expressions (8) and (30)-(35), for the case of isotropic FGPs, the edge displacements and forces vectors may be written as the following:

$$\{d_n\}=\{\bar{d}_n\}\left(e^{ik_n y}-e^{-ik_n y}\right)e^{i\omega t} \quad (36)$$

$$\{p_n\}=\{\bar{p}_n\}\left(e^{ik_n y}-e^{-ik_n y}\right)e^{i\omega t} \quad (37)$$

where

$$\{\bar{d}_n\}=[X_n]\begin{Bmatrix}\tilde{A}_{1n}\\ \tilde{A}_{2n}\\ \tilde{B}_{1n}\\ \tilde{B}_{2n}\\ \tilde{C}_{1n}\\ \tilde{C}_{2n}\end{Bmatrix}=[X_n]_{6\times6}\{\Xi\}_{6\times1} \quad (38)$$

$$\{\bar{p}_n\}=[Y_n]\begin{Bmatrix}\tilde{A}_{1n}\\ \tilde{A}_{2n}\\ \tilde{B}_{1n}\\ \tilde{B}_{2n}\\ \tilde{C}_{1n}\\ \tilde{C}_{2n}\end{Bmatrix}=[Y_n]_{6\times6}\{\Xi\}_{6\times1} \quad (39)$$

Combining Eqs. (38) and (39) by eliminating $\{\Xi\}$, we may have what follows:

$$\{\bar{p}_n\}=[S_n]\{\bar{d}_n\} \quad (40)$$

Where

$$[S_n]=[Y_n][X_n]^{-1} \quad (41)$$

Here, $[S_n]$ is the dynamic stiffness matrix of a component of the plate. Assembling the stiffness matrices of all components of a FGM plate and imposing the boundary conditions, the overall stiffness matrix of the FGM plate is obtained. The exact natural frequencies, ω , for lateral vibration of the plate are extracted by the following equation:

$$\mathrm{Det}\left[S_n(\omega)\right]=0 \quad (42)$$

5. Numerical Results

5.1 General

The following non-dimensional variables are used in the results:

$$\alpha = \frac{L}{b}, \beta = \frac{h}{L}, \Omega = \omega h \sqrt{\frac{\rho_t}{E_t}} \quad (43)$$

Where Ω denotes dimensionless natural frequency, and α and β are the aspect ratios of the plate.

In the present method, the parameter *n* determines the number of half-wavelengths along *y*-direction. The symbol *CSF*G, for example, identifies a plate with edges clamped, simply supported, free and guided; start counting counter clockwise from the left edge of the plate.

Table 1 summarizes the mechanical properties of metal and ceramics used in the FGP. According to the literature reviewed in the current study, most researchers use the power-law function as stated in Eqs. (1) and (2) to describe the material properties and volume fraction of the plate. Therefore, in the current study, FGPs with power-law function is considered.

5.2 Validity

To demonstrate the reliability of the present DSM in the analysis of FGPs, the natural frequencies of isotropic *SSSS* plates are compared with those obtained by Reddy [34] using the Mindlin method. The natural frequencies for different aspect ratios β, are shown in Table 2. The shear correction factor is equal to $5/6$. The DSM results are obtained from the first mode *n* = 1 and show a good agreement with the results of Ref. [1].

The natural frequency parameters of the *SSSS* square FGPs $(\alpha = 1)$ for different values of the thickness to length ratios including 0.05, 0.1 and 0.2 are presented in Table 3. The fundamental frequency and the lowest second frequency parameters are given when β = 0.05, 0.1 and 0.2 respectively. The values of power law index *P* are selected as 0, 0.5, 1, 4, 10 and ∞. The plates are made of a mixture of aluminium (Al) and alumina (Al_2O_3). It should be noted that the solutions reported by Hosseini-Hashemi et al. [12] present an exact closed-form procedure for the free vibration analysis of moderately thick rectangular plates based on the Reissner–Mindlin plate theory. As observed in Table 3, the present DSM results are almost the same as those obtained by the FSDT exact closed-form procedure. Zhao et al. [37] employed the FSDT using the element-free *kp*-Ritz method. For simplicity in comparison, we use non-dimensional frequencies Ω. As observed, when β = 0.05, the present exact results are in excellent agreement with those obtained by the numerical method based on the FSDT [37]. It is also seen that the present solution has a good agreement with that obtained by the HSDT [38] for the thicker FG square plates (β =0.1, 0.2), particularly at the higher modes of vibration.

Table 1. The material properties of the FGPs [12]

Material	Properties		
	$E\,(GPa)$	ϑ	$\rho\left(\frac{kg}{m^3}\right)$
Metallic			
Steel (St)	200	0.3	7800
Aluminum (Al)	70	0.3	2702
Ceramic			
Alumina (Al_2O_3)	380	0.3	3800
Zirconia (ZrO_2)	200	0.3	5700

Table 2. The free vibration $(\Omega \times 1000)$ of isotropic simply support plate for different β

$\beta = (h/L)$	Ref. [1]	Present
0.20	209.28	209.27
0.10	56.943	56.943
0.05	14.587	14.588
0.04	9.4032	9.4038
0.02	2.3508	2.3514
0.01	0.5880	0.5828

Table 3. The comparison of the natural frequency parameter for SSSS, Al/Al_2O_3 square plates

β	Mode	Theory	Power-law index (P)					
			0	0.5	1	4	10	∞
0.05	1	Present	0.0148	0.0125	0.0113	0.0098	0.0094	0.0075
		FSDT [12]	0.0148	0.0125	0.0113	0.0098	0.0094	0.0075
		FSDT [37]	0.0146	0.0124	0.0112	0.0097	0.0093	
0.1	1	Present	0.0577	0.0490	0.0442	0.0383	0.0366	0.0294
		FSDT [12]	0.0577	0.0490	0.0442	0.0381	0.0364	0.0293
		FSDT [37]	0.0568	0.0482	0.0435	0.0376	0.0363	-
		HSDT [38]	0.0577	0.0492	0.0443	0.0381	0.0364	0.0393
	2	present	0.1376	0.1173	0.1061	0.0915	0.0869	0.0701
		FSDT [12]	0.1376	0.1174	0.1059	0.0903	0.0856	0.0701
		FSDT [37]	0.1354	0.1154	0.1042	—	0.0850	-
		HSDT [38]	0.1381	0.1180	0.1063	0.0904	0.0859	0.0701
0.2	1	present	0.2112	0.1805	0.1634	0.1405	0.1329	0.1076
		FSDT [12]	0.2112	0.1805	0.1631	0.1397	0.1324	0.1076
		FSDT [37]	0.2055	0.1757	0.1620	0.1371	0.1304	-
		HSDT [38]	0.2121	0.1819	0.1640	0.1383	0.1306	0.1077
	2	present	0.4618	0.3981	0.3616	0.3078	0.2874	0.2351
		FSDT [12]	0.4618	0.3978	0.3604	0.3049	0.2856	0.2352
		HSDT [38]	0.4658	0.4040	0.3644	0.3000	0.2790	0.2365

5.3 Numerical Results and Discussion

Some cases of FGPs with different boundary conditions are considered in this study. The material properties of FGPs are introduced in Table 1.

The stiffness matrix components are transcendental functions of the eigenvalues. The well-known Wittrick–Williams algorithm [31] may be used to solve this nonstandard eigenvalue problem. Here, a trial-and-error procedure is used to derive the natural frequencies from the eigen function of the plate presented in Eq. (42). Fig. 6 shows the variation of determinant of $S_n(\omega)$ in logarithmic scale with respect to the free vibration frequency ω. The natural frequency ω of the simply-supported square FGPs $(\alpha=1)$ for the thickness to length ratio of $\beta=0.2$ and the power law index of $P=4.0$ are also presented in this figure. The values of the natural frequencies are shown as ω_i^n where n is the wave number in the y–direction for the ith mode. As shown in Fig. 6, the first and the second natural frequencies of this case are derived from one half wave in the y–direction and their values are ω_1^1=7200 radians/sec (Ω_1^1=0.1405) and ω_2^1=15400 radians/sec $\left(\Omega_2^1=0.3078\right)$ respectively as listed in Table 3. Also, the third frequency is associated with two half waves in the y–direction ($n=2$).

To demonstrate the effect of volume fraction on the free vibration, the first six natural frequencies of the FGP with SSSS boundary condition $(\alpha=1,\beta=0.2)$ are presented in Fig. 7. The first and second natural frequencies are compared with those obtained by an exact analytical approach [12]. The method developed in the present study and the one presented in Ref. [12] are both exact solutions of the differential equations of motion for the moderately thick FGP, thus the results are the same. It can be implied from Fig. 7 that increasing power-law index, P, results in decreasing the frequency of all modes. In simply-supported boundary condition (SSSS), the second and the third frequency parameters of a FG square plate are equal for every power-law index. Similarly, the frequencies of fifth and sixth modes of vibration are the same (as shown in Fig. 7). To explain the reason of this matter, mode shapes of the first six modes of vibration are presented in Fig. 8.

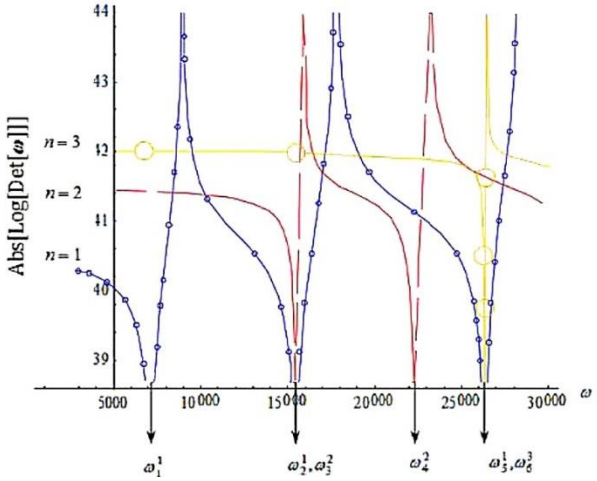

Figure 6. The overall stiffness matrix determinant with respect to the frequency parameter

As it can be seen in Fig. 8b, the second mode corresponds to n = 1, which means there is one half sinusoidal wave along y-direction. In this mode, the plate experiences two half sinusoidal waves along x-direction. On the other hand, the third mode of Fig. 8c happened corresponds to n = 2 which means there are two half sinusoidal waves along y-direction. In this mode, the plate experiences one half sinusoidal wave along x-direction. As the vibration is relevant to a SSSS square plate, there is symmetry with respect to x and y axes. Thus, the second and third modes create similar mode shapes, and they have the same frequencies. A similar symmetry exists between fifth and sixth modes (see Fig. 8e and 8f).

The first three dimensionless frequencies (eigenvalues) of the FGP with Simply-Clamped (SSSC), Simply-Simply (SSSS), Clamped-Guided (SCSG) and Simply-Guided (SSSG) boundary conditions are given in Table 4 for different values of the power law index P, as 0, 0.5, 1, 10 and ∞. A squared shape plate is considered $(\alpha = 1)$ with three different thickness to length ratios including 0.05 (corresponding to thin plates), 0.1 and 0.2 (corresponding to moderately thick plates).

It is found that when the power-law index increases, the frequencies decrease for all boundary conditions. As it is expected, among these four boundary conditions, the maximum and minimum natural frequencies are according to SSSC and SSSG, respectively. The frequencies in this table are mainly presented to show the ability of the formulation to solve different FG materials and boundary conditions. These results can be used as a benchmark to evaluate the precision of other analytical or numerical methods.

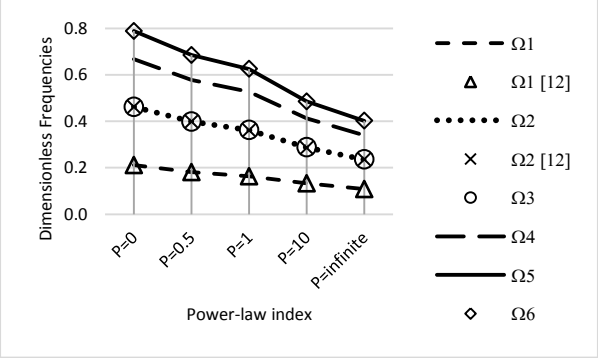

Figure 7. The dimensionless frequencies for the simply-supported (SSSS) moderately thick FGP (β =0.2)

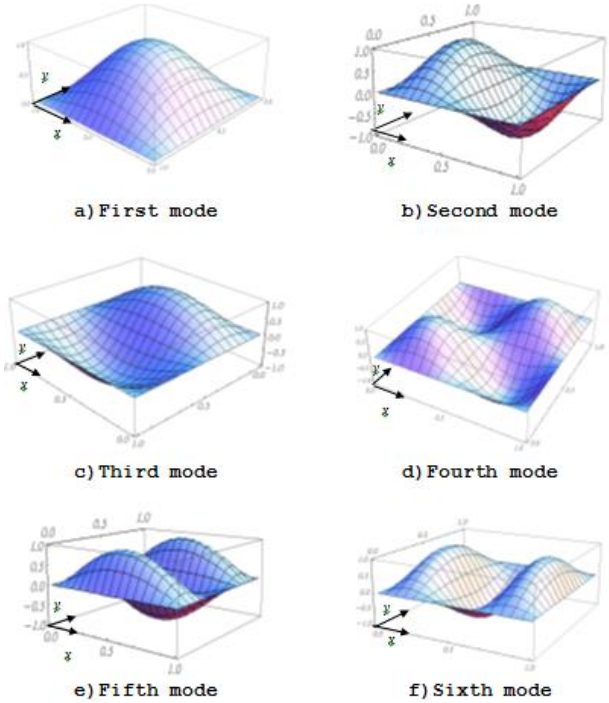

Figure 8. The first Six mode shapes for free vibration of the simply supported (SSSS) moderately thick FGP

6. Conclusion

In this investigation, a dynamic stiffness method for free vibration analysis of moderately thick functionally graded material plates was developed. Due to the variation of the elastic properties through the thickness, the equations of motion governing the in-plane and transverse deformations were coupled. However, this coupling was due to the arbitrary selection of the mid-plane as the reference plane in the development of plate theories. But we can always find a reference plane in which the out-of-plane displacements are uncoupled from the in-plane displacements, so that the FG plates behave as homogeneous plates. Then, for solving the equations of motion by the DSM, the potential functions were used to convert the three extant out-of-plane equations to three independent equations. Solving these independent equations and composing the results of each equation, the exact stiffness matrix of a plate element was derived and the free vibration frequencies of a moderately thick plate were obtained. Using the method, the results are obtained for different boundary conditions. This study offers a new solution and insight into the effect of various parameters on the free vibration analysis of moderately thick functionally graded material plates.

Table 4. The first three dimensionless frequencies Ω_i of the FGPs for different β and P values and in four boundary conditions

Boundary Conditions	P	$\beta = 0.1$			$\beta = 0.2$		
		Ω_1	Ω_2	Ω_3	Ω_1	Ω_2	Ω_3
SSSS	0	0.0577 (n=1)	0.1376 (n=1)	0.1376 (n=2)	0.2112 (n=1)	0.4618 (n=1)	0.4618 (n=2)
	0.5	0.0490 (n=1)	0.1173 (n=1)	0.1173 (n=2)	0.1805 (n=1)	0.3981 (n=1)	0.3981 (n=2)
	1.0	0.0442 (n=1)	0.1061 (n=1)	0.1061 (n=2)	0.1634 (n=1)	0.3616 (n=1)	0.3616 (n=2)
	10	0.0366 (n=1)	0.0869 (n=1)	0.0869 (n=2)	0.1329 (n=1)	0.2874 (n=1)	0.2874 (n=2)
	∞	0.0294 (n=1)	0.0701 (n=1)	0.0701 (n=2)	0.1076 (n=1)	0.2351 (n=1)	0.2351 (n=2)
SSSC	0	0.06762 (n=1)	0.14222 (n=2)	0.15752 (n=1)	0.23638 (n=1)	0.46858 (n=2)	0.49758 (n=1)
	0.5	0.05757 (n=1)	0.12142 (n=2)	0.13472 (n=1)	0.20318 (n=1)	0.40457 (n=2)	0.43163 (n=1)
	1	0.05202 (n=1)	0.10982 (n=2)	0.12197 (n=1)	0.18436 (n=1)	0.36781 (n=2)	0.39331 (n=1)
	10	0.04282 (n=1)	0.08972 (n=2)	0.09902 (n=1)	0.14760 (n=1)	0.29094 (n=2)	0.30711 (n=1)
	∞	0.03452 (n=1)	0.07252 (n=2)	0.08021 (n=1)	0.12035 (n=1)	0.23861 (n=2)	0.25335 (n=1)
SGSC	0	0.04291 (n=1)	0.11002 (n=1)	0.12761 (n=2)	0.16505 (n=1)	0.36755 (n=1)	0.44565 (n=2)
	0.5	0.03642 (n=1)	0.09324 (n=1)	0.10852 (n=2)	0.14045 (n=1)	0.31965 (n=1)	0.38005 (n=2)
	1	0.03273 (n=1)	0.08432 (n=1)	0.09802 (n=2)	0.12705 (n=1)	0.28811 (n=1)	0.34395 (n=2)
	10	0.02742 (n=1)	0.06982 (n=1)	0.08091 (n=2)	0.10505 (n=1)	0.22849 (n=1)	0.27505 (n=2)
	∞	0.02184 (n=1)	0.05570 (n=1)	0.06502 (n=2)	0.08405 (n=1)	0.18725 (n=1)	0.22495 (n=2)
SSSG	0	0.03902 (n=1)	0.09392 (n=1)	0.12552 (n=2)	0.15311 (n=1)	0.33465 (n=1)	0.43661 (n=2)
	0.5	0.03302 (n=1)	0.08002 (n=1)	0.10673 (n=2)	0.13005 (n=1)	0.28695 (n=1)	0.37517 (n=2)
	1	0.03002 (n=1)	0.07202 (n=1)	0.09632 (n=2)	0.11731 (n=1)	0.26005 (n=1)	0.34045 (n=2)
	10	0.02492 (n=1)	0.06002 (n=1)	0.08002 (n=2)	0.09735 (n=1)	0.20995 (n=1)	0.27285 (n=2)
	∞	0.01985 (n=1)	0.04782 (n=1)	0.06392 (n=2)	0.08005 (n=1)	0.17045 (n=1)	0.22245 (n=2)

Nomenclature

h	the thickness of the structure
p	volume fraction exponent
V_c	volume fraction
T	the material's property
E	the modulus of elasticity
u and v	in-plane displacements
w	the out-of-plane displacement
Q_{ij}	the reduced stiffness components
G	the shear modules
N, M, Q	the vectors of in-plane forces
A_{ij}	the shear stiffness resultants
k_s^2	the shear correction factor
w_1,w_2 and H	potential functions
n	mode in y direction
$[S_n]$	the dynamic stiffness matrix of a component of the plate
ω	the frequency of vibration
$\rho(z)$	the mass density that can potentially vary through the thickness
ψ_1, ψ_2 ,ψ_3	the wave numbers
Ω	dimensionless natural frequency
α and β	the aspect ratios of the plate
ρ	the density
ϑ	the Poisson's ratio
ϕ_x and ϕ_y	the out-of-plane displacements
ε_{xx} ,ε_{yy} ,γ_{xy}	in-plane strains
γ_{xz} ,γ_{yz}	the transverse shear strains

Appendix

Some coefficients referred to in this study are given as follows:

$$\left\{\bar{d}_n\right\}_{6\times 6} =$$

$$\begin{Bmatrix} k_n(2-\sigma_1) & k_n(2-\sigma_1) & k_n(2-\sigma_2) & k_n(2-\sigma_2) & -\mu_n & \mu_n \\ (\sigma_1-1)r_n & -(\sigma_1-1)r_n & (\sigma_2-1)\chi_n & -(\sigma_2-1)\chi_n & -k_n & -k_n \\ 1 & 1 & 1 & 1 & 0 & 0 \\ (k_n(2-\sigma_1))\times e^{r_n b} & (k_n(2-\sigma_1))\times e^{-r_n b} & (k_n(2-\sigma_1))\times e^{\chi_n b} & (k_n(2-\sigma_1))\times e^{-\chi_n b} & -\mu_n\times e^{\mu_n b} & \mu_n\times e^{-\mu_n b} \\ ((\sigma_1-1)r_n)\times e^{r_n b} & -((\sigma_1-1)r_n)\times e^{-r_n b} & ((\sigma_1-1)\chi_n)\times e^{\chi_n b} & -((\sigma_1-1)\chi_n)\times e^{-\chi_n b} & -k_n\times e^{\mu_n b} & -k_n\times e^{-\mu_n b} \\ e^{r_n b} & e^{-r_n b} & e^{\chi_n b} & e^{-\chi_n b} & 0 & 0 \end{Bmatrix} \begin{Bmatrix} \tilde{A}_{1n} \\ \tilde{A}_{2n} \\ \tilde{B}_{1n} \\ \tilde{B}_{2n} \\ \tilde{C}_{1n} \\ \tilde{C}_{2n} \end{Bmatrix}$$

$$\left\{\overline{p}_n\right\}_{6\times 6} =$$

$$\begin{Bmatrix}
2k_n r_n(\sigma_1-1)\times c & -2k_n r_n(\sigma_1-1)\times c \\
D_0'(\sigma_1-1)\left(r_n^2-\vartheta k_n^2\right) & D_0'(\sigma_1-1)\left(r_n^2-\vartheta k_n^2\right) \\
\left(k^2 Ghr_n\sigma_1+2k_n^2 r_n(\sigma_1-1)\times r\right) & -\left(k^2 Ghr_n\sigma_1+2k_n^2 r_n(\sigma_1-1)\times c\right) \\
\left(2k_n r_n(\sigma_1-1)\times c\right)\times e^{r_n b} & \left(-2k_n r_n(\sigma_1-1)\times c\right)\times e^{-r_n b} \\
\left(D_0'(\sigma_1-1)\left(r_n^2-\vartheta k_n^2\right)\right)\times e^{r_n b} & \left(D_0'(\sigma_1-1)\left(r_n^2-\vartheta k_n^2\right)\right)\times e^{-r_n b} \\
\left(k^2 Ghr_n\sigma_1+2k_n^2 r_n(\sigma_1-1)\times c\right)\times e^{r_n b} & -\left(k^2 Ghr_n\sigma_1+2k_n^2 r_n(\sigma_1-1)\times c\right)\times e^{-r_n b} \\
2k_n\chi_n(\sigma_2-1)\times c & -2k_n\chi_n(\sigma_2-1)\times c \\
D_0'(\sigma_2-1)\left(\chi_n^2-\vartheta k_n^2\right) & D_0'(\sigma_2-1)\left(\chi_n^2-\vartheta k_n^2\right) \\
\left(k^2 Gh\chi_n\sigma_2+2k_n^2\chi_n(\sigma_2-1)\times c\right) & -\left(k^2 Gh\chi_n\sigma_2+2k_n^2\chi_n(\sigma_2-1)\times c\right) \\
\left(2k_n\chi_n(\sigma_2-1)\times c\right)\times e^{\chi_n b} & \left(-2k_n\chi_n(\sigma_2-1)\times c\right)\times e^{-\chi_n b} \\
\left(D_0'(\sigma_2-1)\left(\chi_n^2-\vartheta k_n^2\right)\right)\times e^{\chi_n b} & \left(D_0'(\sigma_2-1)\left(\chi_n^2-\vartheta k_n^2\right)\right)\times e^{-\chi_n b} \\
\left(k^2 Gh\chi_n\sigma_2+2k_n^2\chi_n(\sigma_2-1)\times c\right)\times e^{\chi_n b} & -\left(k^2 Gh\chi_n\sigma_2+2k_n^2\chi_n(\sigma_2-1)\times c\right)\times e^{-\chi_n b} \\
\left(-k_n^2+\mu_n^2\right)\times c & \left(-k_n^2+\mu_n^2\right)\times c \\
-D_0'k_n\mu_n(1+\vartheta) & D_0'k_n\mu_n(1+\vartheta) \\
\left(-k_n k^2 Gh-k_n^3+k_n\mu_n^2\right) & \left(-k_n k^2 Gh-k_n^3-k_n\mu_n^2\right) \\
\left(-k_n^2+\mu_n^2\right)\times c\times e^{\mu_n b} & \left(-k_n^2+\mu_n^2\right)\times c\times e^{-\mu_n b} \\
-D_0'k_n\mu_n(1+\vartheta)\times e^{\mu_n b} & D_0'k_n\mu_n(1+\vartheta)\times e^{-\mu_n b} \\
\left(-k_n k^2 Gh-k_n^3+k_n\mu_n^2\right)\times e^{\mu_n b} & \left(-k_n k^2 Gh-k_n^3-k_n\mu_n^2\right)\times e^{-\mu_n b}
\end{Bmatrix}
\begin{Bmatrix}
\tilde{A}_{1n} \\ \tilde{A}_{2n} \\ \tilde{B}_{1n} \\ \tilde{B}_{2n} \\ \tilde{C}_{1n} \\ \tilde{C}_{2n}
\end{Bmatrix}$$

Where $c=\left(D_0'\dfrac{1-\vartheta}{2}\right)$. For simplicity, ϑ is assumed to be constant.

References

[1] Mizuguchi F, Ohnabe H. Large deflections of heated functionally graded clamped rectangular plates with varying rigidity in thickness direction. *4th Int Symp Funct Graded Mater*, AIST Tsukuba Research Center, Tsukuba, Japan, 1996; 81-86.

[2] Praveen GN. Reddy JN. Nonlinear transient thermoelastic analysis of functionally graded ceramic-metal plates. *Int J Solids Struct* 1998; 35(33): 4457-4476.

[3] Yang J. Shen HS. Dynamic response of initially stressed functionally graded rectangular thin plates. *Compos Struct* 2001; 54(4): 497-508.

[4] Yang J. Shen HS. Vibration characteristics and transient response of shear deformable functionally graded plates in thermal environments. *J Sound Vib* 2002; 255(3): 579-602

[5] Ma LS. Wang TJ. Relationships between axisymmetric bending and buckling solutions of FGM circular plates based on third-order plate theory and classical plate theory. *Int J Solids Struct* 2004; 41(1): 85-101.

[6] Kitipornchai S. Yang J. Liew KM. Semi-analytical solution for nonlinear vibration of laminated FGM plates with geometric imperfections. *Int J Solids Struct* 2004; 41(9-10): 2235-2357.

[7] Najafizadeh MM. Heydari HR. Thermal buckling of functionally graded circular plates based on higher order shear deformation plate theory. *Eur J Mech - A/Solids* 2004; 23(6): 1085-1100.

[8] Bian ZG. Chen WQ. Lim CW. Zhang N. Analytical solutions for single- and multi-span functionally graded plates in cylindrical bending. *Int J Solids Struct* 2005; 42(24-25): 6433-6456.

[9] Chen, WQ. Bian ZG. Ding HJ. Three-dimensional vibration analysis of fluid-filled orthotropic FGM cylindrical shells. *Int J Mech Sci* 2004; 46(1): 159-171.
[10] Wu L. Liu J. Free vibration analysis of arbitrary shaped thick plates by differential cubature method. *Int J Mech Sci* 2005; 47(1): 63-81.
[11] Abrate S. Free vibration, buckling and static deflections of functionally graded plates. *Compos Sci Technol* 2006; 66(14): 2383–2394.
[12] Hosseini-Hashemi Sh. Fadaee M. Atashipour SR. A New Exact Analytical Approach for Free Vibration of Reissner–Mindlin Functionally Graded Rectangular Plates. *Int J Mech Sci* 2010; 53(1): 11-22.
[13] Hosseini-Hashemi Sh. Rokni Damavandi Tahar H. Akhavan H. Omidi M. Free vibration of functionally Graded rectangular plates using first-order shear deformation plate theory. *Appl Math Modell* 2010; 34(5): 1276-91.
[14] Prakash T. Ganapathi M. Asymmetric flexural vibration and thermoelastic stability of FGM circular plates using finite element method. *Compos Part B: Eng* 2006; 37(7-8): 642-649.
[15] Shariyat M. Vibration and dynamic buckling control of imperfect hybrid FGM plates with temperature-dependent material properties subjected to thermo-electro-mechanical loading conditions. *Compos Struct* 2009; 88(2): 240-252.
[16] Afsar AM. Go J. Finite element analysis of thermoelastic field in a rotating FGM circular disk. *Appl Math Modell* 2010; 34(11): 3309-3320.
[17] Prakash T. Singha MK. Ganapathi M. A finite element study on the large amplitude flexural vibration characteristics of FGM plates under aerodynamic load*. Int J Non-Linear Mech* 2012; 47(5): 439-447.
[18] Leung AYT. Fung TC. Non-linear vibration of frames by the incremental dynamic stiffness method. *Int J Numer Methods Eng* 1990; 29(2): 337-356.
[19] Banerjee JR. Dynamic stiffness formulation for structural elements: A general approach. *Comput Struct* 1995; 63(1): 101-103.
[20] Bercin AN. Analysis of orthotropic plate structures by the direct -dynamic stiffness method. *Mech Res Commun* 1995; 22(5): 461-466.
[21] Bercin AN. Langley RS. Application of the dynamic stiffness technique to the in-plane vibrations of plate structures. *Comput Struct* 1996; 59(5): 869-875.
[22] Bercin AN. Analysis of energy flow in thick plate structures. *Comput Struct* 1997; 62(4): 747-756.
[23] Bercin AN. Eigenfrequencies of rectangular plate assemblies. *Comput Struct* 1997; 65(5): 703-711.
[24] Birgersson F. Ferguson NS. Finnveden S. Application of the spectral finite element method to turbulent boundray layer induced vibration of plates. *J Sound Vib* 2003; 259(4): 873-891.
[25] Hatami S. Azhari M. Dynamic stiffness analysis of orthotropic plates moving on some rollers and an elastic foundation*, 7th Int Congr Civil Eng***.** Tarbiat Modarres University, 2006; 20-22*,:*
[26] Boscolo M. Banerjee JR. Dynamic stiffness elements and their applications for plates using first order shear deformation theory. *Comput Struct* 2011; 89(3-4): 395-410.
[27] Boscolo M. Banerjee JR. Dynamic stiffness formulation for composite Mindlin plates for exact modal analysis of structures. Part I: Theory. *Comput Struct* 2012; 96-97: 61-73.
[28] Boscolo M. Banerjee JR. Dynamic stiffness method for exact in-plane free vibration analysis of plates and plate assemblies. *J Sound Vib* 2011; 330(12): 2928-36.
[29] Boscolo M. Banerjee JR. Dynamic stiffness formulation for composite Mindlin plates for exact modal analysis of structures. Part II: Results and applications. *Comput Struct* 2012; 96-97: 74-83.
[30] Fazzolari FA. Boscolo M. Banerjee JR. An exact dynamic stiffness element using a higher order shear deformation theory for free vibration analysis of composite plate assemblies. *Compos Struct* 2013; 96: 262-278.
[31] Wittrick WH. Williams FW. A general algorithm for computing natural frequncies of elastic structures. *J Mech Appl Math* 1971; 24(3): 263-284.
[32] Nefovska-Danilovic M. Petronijevic M. In-plane free vibration and response analysis of isotropic rectangular plates using the dynamic stiffness method. *Comput Struct* 2015; 152: 82-95.
[33] Liu X. Banerjee JR. Free vibration analysis for plates with arbitrary boundary conditions using a novel spectral-dynamic stiffness method. *Comput Struct* 2016; 164: 108-126
[34] Reddy JN. **Theory and analysis of elastic plates and shells**, New York: CRC Taylor & Francis Group; 2007.
[35] Abrate S. Functionally graded plates behave like homogeneous plates. *Compos Part B: Eng* 2008; 39(1): 151-158.

[36] Mindlin RD. Influence of rotary inertia and shear on flexural motions of isotropic, elastic plates. *J Appl Mech* 1951; 18: 31-38.
[37] Zhao X. Lee Y. LiewK. Free vibration analysis of functionally graded plates using the element-free kp-Ritz method. *J Sound Vib* 2009; 918-39.
[38] Matsunaga H. Free vibration and stability of functionally graded plates according to a 2-D higher-order deformation theory. *Compos Struct* 2008; 319(3-5): 499-512.